Applied Catalysis B: Environmental 174–175 (2015) 193–202

Contents lists available at ScienceDirect

Applied Catalysis B: Environmental

journal homepage: www.elsevier.com/locate/apcatb

Dramatic enhancement of visible light photocatalysis due to strong interaction between TiO_2 and end-group functionalized P3HT

Jianling Zhang, Haigang Yang, Shoubin Xu, Long Yang, Yuanqing Song, Long Jiang*, Yi Dan*

State Key Laboratory of Polymer Materials Engineering of China (Sichuan University), Polymer Research Institute of Sichuan University, Chengdu 610065, China

ARTICLE INFO

Article history:
Received 30 December 2014
Received in revised form 23 February 2015
Accepted 25 February 2015
Available online 27 February 2015

Keywords:
P3HT/TiO_2 composites
Interfacial interaction
Photocatalytic activity
End-group functionalized P3HT

ABSTRACT

Conjugated polymer/TiO_2 photocatalysts hold great promise for solar chemical conversion processes by combining the advantages from both the conjugated polymer and the inorganic semiconductor, overcoming the serious drawbacks of fast charge recombination and the limited visible light absorption of inorganic semiconductor through interfacial electron transfer. To address the crucial way to promote the visible light photocatalytic activity of conjugated polymers/TiO_2 photocatalysts, P3HT/TiO_2 composites with strong interfacial interaction between P3HT and TiO_2, which was demonstrated by the results of X-ray photoelectron spectroscopy and dissolution tests, were prepared by binding cyanoacrylic acid end-groups functionalized P3HT to the surface of TiO_2. The pseudo-first-order kinetic constants of photocatalytic degradation of model pollutant methyl orange (MO) under visible light with P3HT/TiO_2 composites of monofunctionalized and difunctionalized polymers were 7.06 and 20.18 times as great as that of unfunctionalized polymer, respectively, indicating a remarkably enhanced visible light photocatalytic activities by an order of magnitude with the incorporation of cyanoarrylic acid end-groups. In consideration of their similar morphology, specific surface area, ability of harvesting visible light and adsorption capacities toward MO independent of end-group functionalization, the dramatically enhanced photocatalytic activity arises from the facilitated electron injection and separation of photogenerated carriers owing to strong interfacial interaction between TiO_2 and end-group functionalized P3HT, which was proved to be crucial for photocatalytic capability of conjugated polymer/TiO_2 photocatalysts, providing a new effective direction for the improvement of their visible light photocatalytic activity.

1. Introduction

Semiconductor photocatalysts, which can use solar light to drive many kinds of redox chemical reactions, such as water splitting [1–4] and pollutant degradation [5–7], have attracted considerable attention due to the growing global energy crisis and environmental problems [8,9]. Especially, TiO_2 photocatalysts, with low cost, good biocompatibility and high reactivity, have demonstrated successful performances in degrading a wide variety of organic compounds in water and air under UV illumination [5–7,10]. However, the practical application of TiO_2 photocatalysts is hindered by the lack of visible light activity and low quantum yield [11]. Recently, polymers with extended π-conjugated systems have attracted great interest due to their high absorption coefficients in the visible light region [12–14]. Their tunable optical bandgaps [15,16], easy modified structure [17,18] and high mobility of charge carriers [19] can potentially lead to high light-harvesting efficiency and charge injection efficiency at the interfacial of a wide-bandgap semiconductor [20]. Combining the advantages from both the conjugated polymer and the inorganic semiconductor, conjugated polymer/TiO_2 hybrids may offer a promising future for photocatalysts [21]. Polythiophenes [22–25], polypyrroles [26,27], polyanilines [28–30] and their derivates [31–35] have been widely incorporated with TiO_2, resulting in hybrid photocatalysts with not only efficient visible light activity but also improved ultraviolet light activity by extending the response spectrum of TiO_2 to visible light region and facilitating the separation of photogenerated carriers.

The photocatalytic activity of conjugated polymer/TiO_2 photocatalysts under visible light is due to the visible light absorption of conjugated polymers and the followed electron transfer from the excited polymers to the conduction band (CB) of TiO_2. Efficient charge transfer between the conjugated polymer and the

* Corresponding authors. Tel.: +86 28 85407286; fax: +86 28 85402465.
E-mail addresses: jianglong@scu.edu.cn (L. Jiang), danyichenweiwei@163.com (Y. Dan).

http://dx.doi.org/10.1016/j.apcatb.2015.02.034
0926-3373/

TiO_2, which is a crucial factor for the photocatalytic capability of the composites, is strongly affected by the way of their combination and the strength of the interfacial interaction. Summarizing the findings, so far we have observed that the reported conjugated polymer/TiO_2 photocatalysts have been mostly prepared by physic blending and in situ polymerization while there are mainly weak physical interactions for the composites. It has been reported that strong interfacial interaction resulted from covalent bond can potentially facilitate the electron injection from excited polymers to TiO_2 and enhance the interfacial charge-transfer efficiency [36–38]. Also, dye molecules are generally bound covalently to the semiconductor surface, which has been reported to enable strong electronic coupling interaction between them and facilitate the efficient electron injection process for photovoltaics applications [39,40]. However, it has not been attracted much more attention to map the effect of interfacial interaction on the photogenerated carriers separation of conjugated polymer/TiO_2 photocatalysts and how much they devote to their photocatalytic capability, which is of significant to provide theoretical guidance for the design of new effective photocatalysts.

Thus, our strategy here is to anchor conjugated polymer onto the TiO_2 by covalent bond to improve the interaction between them, expecting that the resulted strong interaction will be favorable for electron injection and photogenerated carriers separation, finally promoting the visible light photocatalytic activity of the photocatalyst. The most popular anchoring groups include carboxylate [15,16,18,41], phosphonate [42–45], silane [46–49], and so on, while cyanoacrylic acid group has been widely utilized and shown to bind efficiently to TiO_2 [39,41]. The anchoring groups can be incorporated in conjugated polymers either by side-chain functionalization or end-group functionalization. Compared to side-chain functionalization, end-group functionalization of conjugated polymers will not lead to unwanted twisting of the polymer chain and a decrease in the effective π-conjugation. In order to focus on the effect of interfacial interaction on the photocatalytic performance of conjugated polymer/TiO_2 photocatalysts and rule out other factors maybe related, in this context, we prepared P3HT/TiO_2 composites with strong interaction between P3HT and TiO_2 by incorporating cyanoacrylic acid groups (one and two) to the end of the regioregular P3HT, which was subsequently bound to the surface of TiO_2, resulting in C1–C3, correspondingly (Scheme 1). We expect that the photocatalytic capability of the resulted composites under visible light will be improved significantly.

2. Experimental

2.1. Materials

3-Hexylthiophene, phosphorus oxychloride were purchased from Chengdu Aike Chemical Technology Co., Ltd. *tert*-Butylmagnesium chloride, *n*-butyllithium and cyanoacetic acid were obtained from Aladdin (Shanghai, China). *N*-Bromosuccinimide (NBS), Ni(dppp)Cl_2, piperidine and methyl orange (MO) were all bought from Kelong Chemical Reagents Factory (Chengdu, China). Titanium dioxide was obtained from Degussa (P25 TiO_2, particle diameter 20 nm, surface area 50 m^2/g). Solvents were dried over appropriate conditions and then distilled. All reagents were used without further purification unless stated otherwise.

2.2. Instrumentation

^1H NMR spectra were recorded on a Bruker Avance II-400 MHz specteometer. Gel permeation chromatography (GPC) analyses were carried out on a Shimadzu 20AD instrument. FTIR spectra were measured on a Nicolet 560 FTIR spectrometer, using KBr as reference sample. UV–vis absorption spectra were recorded on a UV-2300 spectrophotometer (Hitachi, Japan). Fluorescence spectra were measured on an F-4600 spectrometer (Hitachi, Japan). UV–vis diffuse reflectance spectra were recorded on a TU-1901 spectrophotometer equipped with an integrating sphere attachment (IS 19-1). X-ray photoelectron spectroscopy measurements were carried out with a XSAM-800 spectrometer (KRATOS, Britain). High-resolution transmission electron microscopy study was carried out on a Tecnai G2 F20 electron microscopy instrument (FEI, America). The specific surface areas were analyzed by a Quadradorb SI specific surface area and pore size analyzer (Quantachrome, America).

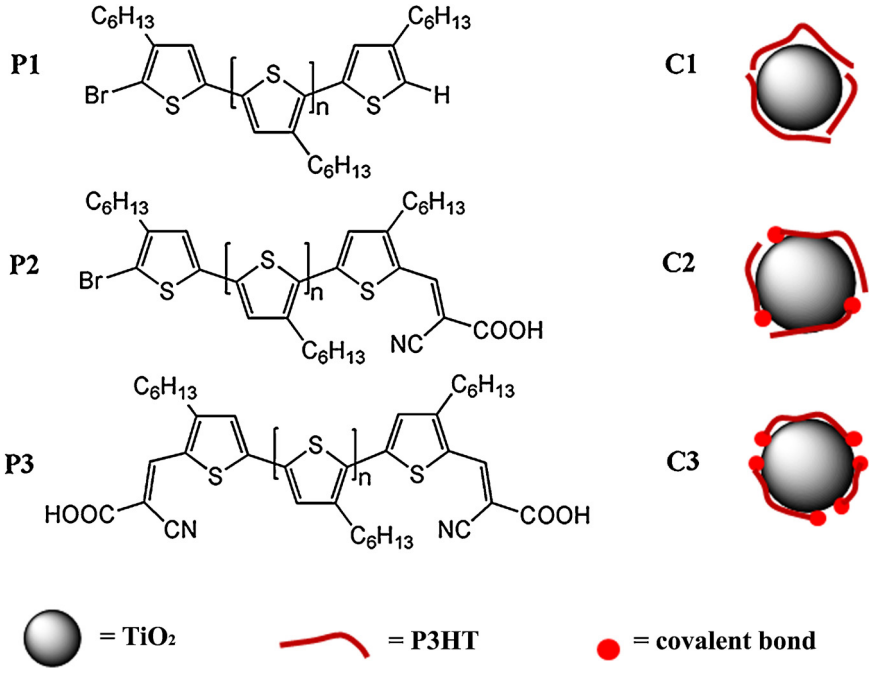

Scheme 1. Structures of P1–P3 and schematic diagram of C1–C3.

2.3. Synthesis and characterization

All reactions were carried out in dry glassware and under argon using Schlenk techniques. 2,5-dibromo-3-hexylthiophene was prepared by using NBS as the brominating reagent adapted from Loewe et al. [50]. Further synthetic procedures were described as follows.

P1: P1 was synthesized by the Grignard metathesis polymerizaition (GRIM) developed by Loewe et al. [50]. *tert*-Butylmagnesium chloride in THF (6.70 mL, 1 M) and 2,5-dibromo-3-hexylthiophene (2 g, 6.13 mmol) were added to 50 mL dry THF in sequence and the mixture was heated to 60 °C to reflux 3 h under atmosphere of argon. Ni(dppp)Cl_2 (55.2 mg, 0.10 mmol) was added after the mixture was cooled to room temperature. After stirred for 12 h, hydrochloric acid was added to terminate the reaction and the solvet was removed by rotary evaporation. The obtained precipitate was redissolved in chloroform, precipitated in methanol and further extracted with methanol to obtain product P1.

GPC: M_n = 15900 g mol^{-1}, M_w = 24100 g mol^{-1}, polydispersity index (PDI) = 1.52, regularity = 89%. ^{1}H NMR (400 MHz, $CDCl_3$): δ = 6.98 (1H, s, H_{ar}), 2.80 (2H, t, α-CH_2), 2.58 (2H, t, α-CH_2 of hydrogen terminated end-group), 1.78–1.53 (2H, m, β-CH_2), 1.48–1.23 (6H, m, CH_2), 1.0–0.75 (3H, m, CH_3).

P1–CHO: P1–CHO was synthesized according to the literature [51]. DMF (1 mL) and $POCl_3$ (1 mL) were added to a solution of P1 (100 mg) in dry toluene (50 mL) under argon. The mixture was heated to 75 °C for 24 h before it was cooled to temperature, quenched with a saturated aqueous solution of sodium acetate (2 mL) and precipitated in methanol (100 mL). After being filtered, the resulting precipitate was Soxhlet-extracted with methanol and subsequently with chloroform under argon. The chloroform was removed by evaporation to give P1–CHO.

^{1}H NMR (400 MHz, $CDCl_3$): δ = 10.02 (1H, s, CHO), 6.98 (1H, s, H_{ar}), 2.80 (2H, t, α-CH_2), 1.78–1.53 (2H, m, β-CH_2), 1.48–1.15 (6H, m, CH_2), 0.99–0.78 (3H, m, CH_3).

P2: P2 was synthesized according to the literature [51]. Under argon, piperidine (0.16 mL, 1.60 mmol) and cyanoacetic acid (0.16 g, 1.85 mmol) were added to a solution of P1–CHO (100 mg) in dry chloroform (30 mL). The mixture was refluxed at 55 °C for 24 h, cooled to room temperature and poured into diluted HCl (pH 3.5). The combined chloroform layers were washed with water to be neutral, dried with sodium sulfate and evaporated to dryness. The residue was redissolved in 5 mL hot toluene and precipitated in methanol (75 mL methanol containing 0.25 mL concentrated HCl). After collected by filtration, the precipitate was Soxhlet-extracted with methanol and then with chloroform under argon. The product was obtained after chloroform was evaporated.

^{1}H NMR (400 MHz, $CDCl_3$): δ = 8.42 (2H, s, H_{vinyl}), 6.98 (1H, s, H_{ar}), 2.80 (2H, t, α-CH_2), 1.78–1.50 (2H, m, β-CH_2), 1.49–1.15 (6H, m, CH_2), 0.97–0.77 (3H, m, CH_3).

CHO–P1–CHO: CHO–P1–CHO was synthesized according to the literature [51]. Under argon, a solution of *N*-butyllithium in hexanes (2.10 mL, 1 M) was added to a solution of P1 (100 mg) in dry THF (30 mL) which was cooled to 0 °C. The mixture was stirred for 40 min and then water was added to terminate the reaction. After evaporated to dryness, redissolved in chloroform, washed with water to be neutral, dried with sodium sulfate and evaporated to dryness again, the remaining residue was dissolved in toluene (80 mL) under argon, in which DMF (1.5 mL) and $POCl_3$ (1.5 mL) were added. The mixture was heated to 75 °C for 24 h before it was cooled to temperature, quenched with a saturated aqueous solution of sodium acetate (2 mL) and precipitated in methanol (100 mL). The resulting precipitate gained by filteration was Soxhlet-extracted with methanol and subsequently with chloroform under argon. After evaporated to dryness, CHO–P1–CHO was obtained.

^{1}H NMR (400 MHz, $CDCl_3$): δ = 10.02 (1H, s, CHO), 6.98 (1H, s, H_{ar}), 2.80 (2H, t, α-CH_2), 1.78–1.53 (2H, m, β-CH_2), 1.48–1.05 (6H, m, CH_2), 0.98–0.75 (3H, m, CH_3).

P3: P3 was synthesized according to the literature [51]. CHO–P1–CHO (60 mg) was dissolved in dry chloroform (30 mL) before piperidine (0.30 mL, 3.0 mmol) and cyanoacetic acid (0.3 g, 3.5 mmol) were added under argon. After refluxed at 55 °C for 24 h, the mixture was cooled to room temperature, poured into diluted HCl (pH 3.5), washed with water to be neutral, dried with sodium sulfate and evaporated to dryness. The residue was redissolved in 5 mL hot toluene and precipitated in methanol (60 mL methanol containing 0.2 mL concentrated HCl). The collected precipitate by filtration was Soxhlet-extracted with methanol and then with chloroform under argon. The product was obtained after chloroform was evaporated.

^{1}H NMR (400 MHz, $CDCl_3$): δ = 8.42 (2H, s, H_{vinyl}), 6.98 (1H, s, H_{ar}), 2.80 (2H, t, α-CH_2), 1.78–1.50 (2H, m, β-CH_2), 1.47–1.17 (6H, m, CH_2), 0.96–0.79 (3H, m, CH_3).

2.4. Preparation of P3HT/TiO_2 composites and evaluation of photocatalysis

The P3HT/TiO_2 composites were prepared by the following procedure: a mount of P3HT chloroform solution was added to the TiO_2 suspension. The mixture was sonicated for 2 h in the dark before the solvent was removed by rotary evaporation under vacuum. After dried in an oven at 40 °C under vacuum for 12 h, the obtained composites were labeled as C1–C3, correspondingly.

The photocatalytic activities of the composites and TiO_2 were studied by the degradation of MO. 100 mg of photocatalyst and MO aqueous solution (200 mL, 10 mg/L) were added to a 500-mL beaker which was surrounded by circulated water to keep temperature at 15 °C. A 500 W tungsten–halogen lamp (OSRAM, Germany), used as the VL irradiation source, was positioned over the solution to

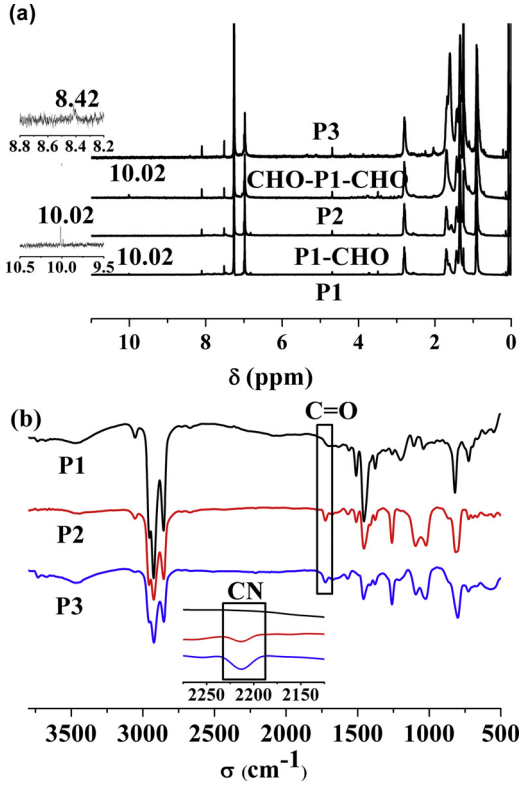

Fig. 1. (a) ^{1}H NMR (400 MHz) spectra of P1, P1–CHO, P2, CHO–P1–CHO and P3. (b) FTIR spectra of P1–P3.

maintain on irradiance of 19 mW/cm^2 while a 420 nm cut-off filter was used to cut off UV light below 420 nm. Before illumination, the suspension was stirred in the dark for 1 h to ensure the establishment of adsorption–desorption equilibrium between the photocatalyst and MO. A portion of the samples were then withdrawn at regular times, filtered immediately for separation of any suspended solid and kept in the dark. The change in the concentration of MO was monitored by measuring the absorbance at λ_{max} (464 nm) with a UV-2300 UV–vis spectrophotometer (Techomp Co., China).

To evaluate the photocatalytic stability of P3HT/TiO_2 composites, the photocatalysts were reused three times as follows. 15 mg of photocatalyst and MO aqueous solution (30 mL, 10 mg/L) were added to a 100 mL beaker which was kept in 15 °C water. To accelerate the photocatalytic reaction, the irradiance was increased from 19 mW/cm^2 to 22 mW/cm^2 compared to photocatalytic experiments above-mentioned. To avoid the loss of photocatalyst, the suspension was stirred in the dark for 1 h and subsequently illuminated for 3 h before centrifugalized to separate photocatalyst from MO solution without samples withdrawn during the photocatalytic reaction. The final decolorization ratio of MO was given by comparing the concentration of MO solution before and after photocatalytic reaction while the photocatalyst was redispersed in a fresh 30-mL MO solution (10 mg/L) to start a new cycle test. After three recycle tests, the photocatalyst was washed by distilled water to remove the remained molecules and dried in a vacuum at 40 °C for 24 h for structure characterization.

3. Results and discussion

3.1. Characterization of P3HT

Highly regioregular P3HT, P1, was synthesized by the Grignard metathesis polymerizaition (GRIM) developed by Loewe et al. [50]. P1 was further functionalized with cyanoacrylic acid by Vilsmerier–Haack formylation (obtaining P1–CHO and CHO–P1–CHO) and subsequent Knoevenagel condensation (obtaining P2 and P3) according to literature [51]. Fig. 1(a) shows ^{1}H NMR (400 MHz) spectra of P1, P1–CHO, P2, CHO–P1–CHO and P3. The appearance of aldehyde proton (10.02 ppm) confirms the successful formylation of P1. The integral ratio of this signal and the signal at 6.98 (β-hydrogen atoms of the thiophene) confirms a quantitative end group. Compared with P1–CHO and CHO–P1–CHO, the signal at ~10 ppm disappears completely for both P2 and P3 and a new signal 8.42 belonging to the vinylic proton appears, indicating an absolutely transformation of aldehyde moieties to cyanoacrylic acid end groups. As displayed in Fig. 1(b), the FTIR spectra of P2 and P3 show two new signals of C=O vibration at 1727 cm^{-1} and C≡N vibration at 2213 cm^{-1}, which are absent in P1, providing further evidence for the successful synthesis of P2 and P3.

Table 1
Optical properties of polymers P1–P3 in solution and film.

Polymer	λ_{max} (nm)		λ_{onset} (nm)/E_g[a] (eV)	
	Solution[b]	Film[c]	Solution[b]	Film[c]
P1	450	513	541/2.29	644/1.92
P2	447	511	543/2.28	655/1.89
P3	440	493	549/2.26	658/1.88

[a] $E_g = 1240/\lambda_{onset}$.
[b] In chlorobenzene.
[c] Spin-coated from chlorobenzene solutions on quartz.

UV–vis absorption spectroscopy was employed to study the optical properties of the end-group functionalized polymers, which are of paramount importance for conjugated polymer/TiO_2 photocatalysts' ability of harvesting light. As shown in Fig. 2(a) and summarized in Table 1, P2 and P3 both exhibit typical π–π^* transition in the range of visible light from 400 nm to 600 nm. Functionatization of one end-group (P2) does not have an obvious effect on the absorption properties, with an onset at 543 nm and a maximum at 547 nm, compared with 541 nm and 550 nm for P1, respectively. However, incorporation of two end-groups results in a red-shifted onset of 8 nm and a blue-shifted absorption maximum of 10 nm. Similarly, P2 film on quartz exhibits typical vibronic bands of π–π stacking, which is nearly the same as P1, while the fine structure is weakened and the maximum absorption is 20 nm blue-shifted in the spectrum of P3. This is because that the two carboxyl acids of P3 can form hydrogen bonds, fix the polymer chain in a disordered conformation and hinder the π–π stacking, resulting in a decrease in the effective conjugation length [18], whereas the single carboxyl acid of P2 has less ability of forming hydrogen bonds. Overall, the optical properties of P1, P2 and P3 are similar and the end-groups have minimal effect on them.

3.2 Characterization of the P3HT/TiO_2 composites

TEM analyses were used to characterize the morphology of P3HT/TiO_2 composites and TiO_2, as presented in Fig. 3. Both TiO_2 and P3HT/TiO_2 composites are composed morphology of globules, with a diameter of about 20 nm. The distance between TiO_2 lattice planes is measured to be 0.349 nm, corresponding to the interplanar spacing of anatase TiO_2 (1 0 1) plane. A polymer layer with the thickness of 1–2 nm can be seen clearly on the surface of TiO_2 for P3HT/TiO_2 composites while no evidently difference can be seen among C1–C3. The surface of photocatalysts plays a great role in the photocatalytic reaction for it is where O_2, H_2O and organic pollutants absorbed and provides active site for the reactions. Therefore, the specific surface areas of TiO_2 and P3HT/TiO_2 composites were obtained by nitrogen gas sorption and the results are listed in

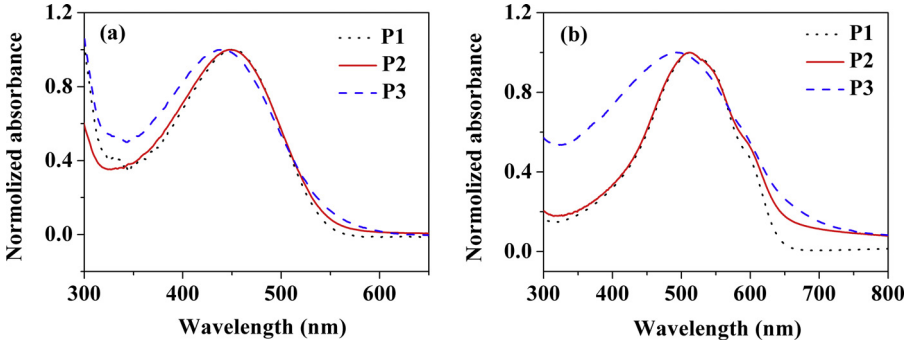

Fig. 2. UV–vis absorption spectra of P1–P3 (a) in chlorobenzene solutions and (b) films on quartz.

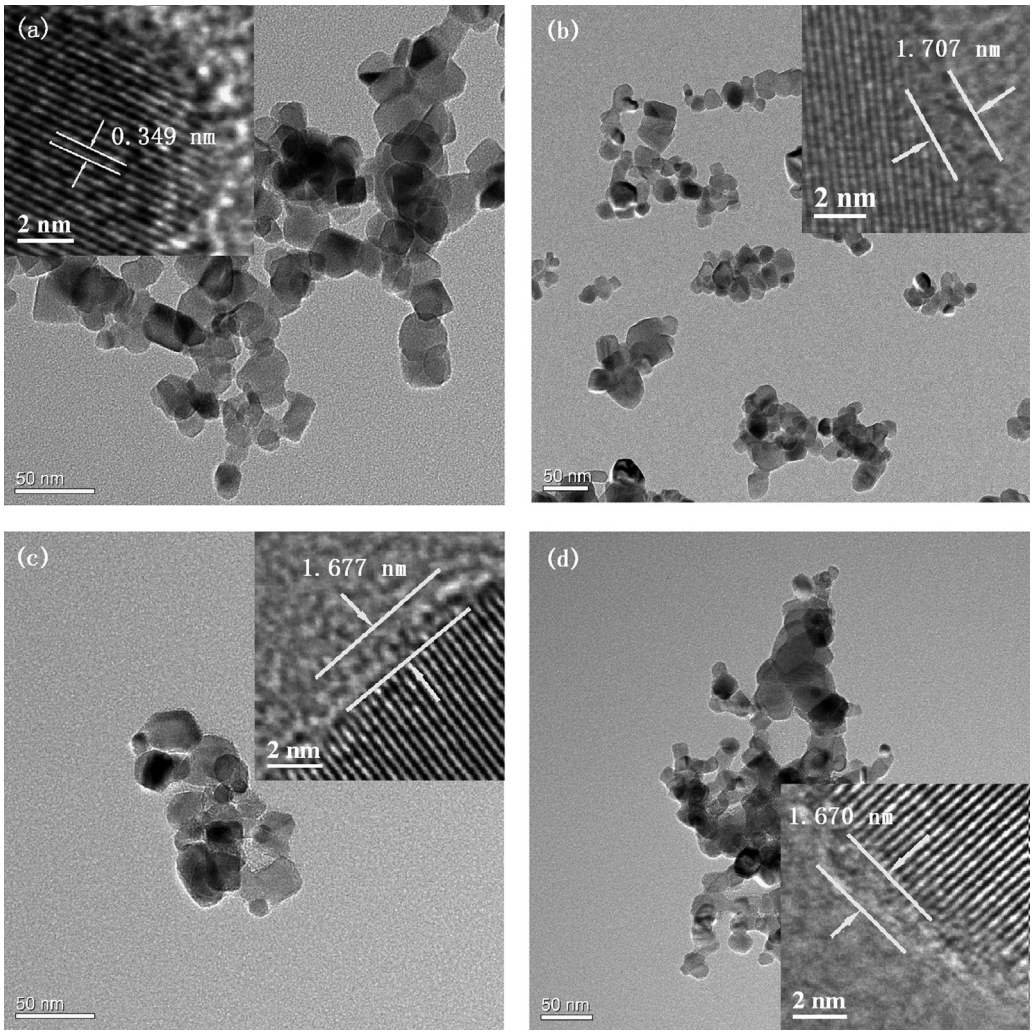

Fig. 3. High-resolution TEM images of (a) TiO_2 and P3HT/TiO_2 composites: (b) C1, (c) C2, and (d) C3.

Table 2
BET surface area (S_{BET}) of TiO_2 and P3HT/TiO_2 composites.

Sample	TiO_2	C1	C2	C3
S_{BET} (m^2/g)	55.1	43.3	43.8	42.5

Table 2. The specific surface areas of C1–C3 are almost the same, a little smaller than that of TiO_2. The decrease in surface area of P3HT/TiO_2 composites can be ascribed to adsorb of P3HT on the surface of TiO_2, which can increase the particles size and block the pores in TiO_2 to some extent.

FTIR spectra of samples were measured to investigate the chemical composition of the prepared samples. As can be seen from Fig. 4, TiO_2 shows strong and broad absorption band at 473 cm^{-1} corresponding to Ti—O—Ti bond and absorption band at 3000–3500 cm^{-1} attributing to —OH groups. The spectra of the composites show not only above absorption bands originating from TiO_2 but also absorption bands at 2956 cm^{-1}, 2925 cm^{-1} and 2855 cm^{-1} belonging to the C—H stretching vibration of hexyl group, which come from the polymers and can be seen in Fig. 1(b), indicating that P3HT/TiO_2 composites composed of P3HT and TiO_2 were successfully prepared. This can be further confirmed by the XPS results for Ti, O, C and S elements were all detected on the surface of P3HT/TiO_2 composites C1–C3.

The high-resolution O1s XPS spectra of P3HT/TiO_2 composites were analyzed to look into the interaction between P3HT and TiO_2 (Fig. 5). For all P3HT/TiO_2 composites, Gaussian-resolved peaks occur at 529.7, 531.5 and 532.7 eV, assigning to Ti—O—Ti, OH on the surface of TiO_2/C=O and OH from the organics/O—C—O, respectively [52–54]. The new peak at 533.8 eV in the O1s spectra of C3, which is not observed for C1 and C2, is a signal of ester bond, suggesting that the P3 binds to TiO_2 by ester bonds through reactions between carboxyl groups of P3 and hydroxyl groups on the surface of TiO_2. This peak is absent in C2 maybe because the number of ester bonds in C2 is less than C3 so that the signal is too weak to be detected.

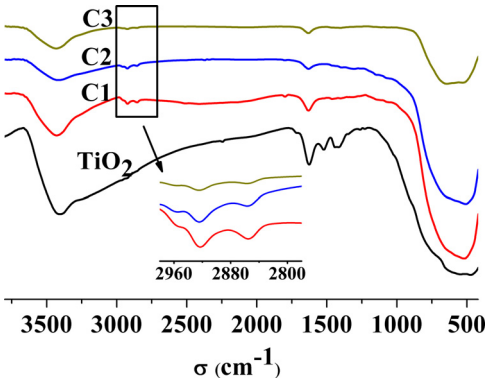

Fig. 4. FTIR spectra of TiO_2 and P3HT/TiO_2 composites.

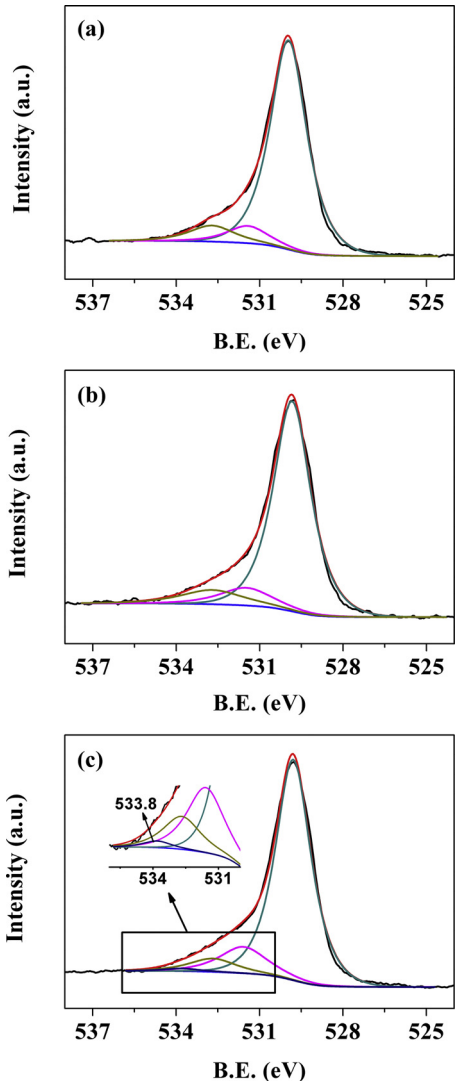

Fig. 5. High resolution XPS spectra of O1s in P3HT/TiO_2 composites: (a) C1, (b) C2 and (c) C3.

The strong interfacial interaction resulted from covalent ether bond can potentially facilitate the electron injection from excited polymers to TiO_2 and enhance the interfacial charge-transfer efficiency [36–38], which is critical to conjugated polymer/TiO_2 photocatalysts.

To give further evidence for the strong interfacial interaction between end-functionalized P3HT (P2 and P3) and TiO_2, 10 mg of P3HT/TiO_2 composites (C1–C3) were added to 5 mL chlorobenzene, respectively, and the mixtures were stirred for 12 h to dissolve polymers from composites. The UV–vis absorption spectra of P3HT solutions dissolved from P3HT/TiO_2 composites are displayed in Fig. 6. The absorbances of dissolved P1–P3 solution for λ_{max} are 0.90, 0.50 and 0.09, which is 10.11, 3.21 and 0.98 times of their solution of 5 mg/L, respectively. P3 was hardly removed from C3 composites while P1 was about totally dissolved from C1 composites and P2 was partly removed from C2 composites, demonstrating that the interfacial interaction strengths between P3HT and TiO_2 follow the order of C3 > C2 > C1, for P1 physisorbed to the TiO_2 while P2, P3 chemisorbed to the TiO_2 and the number of ester bonds in C3 is about 2 times of that in C2.

The visible light absorption of photocatalysts is the first step for the photocatalytic reaction and of vital importance for the photocalytic activity of them. The UV–vis diffuse reflectance spectra,

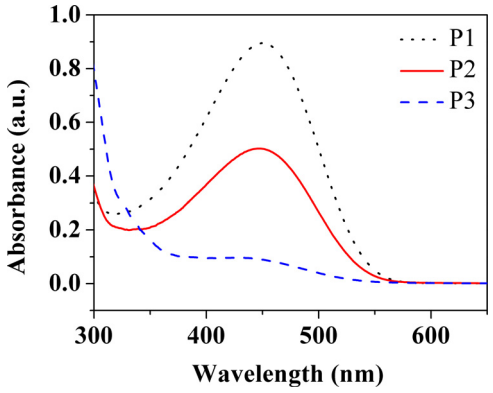

Fig. 6. UV–vis absorption spectra of P3HT solutions dissolved from P3HT/TiO_2 composites.

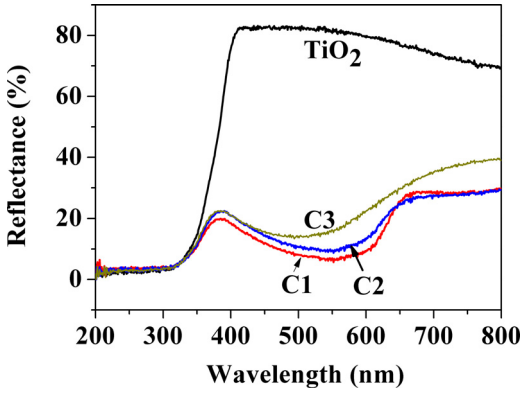

Fig. 7. UV–vis diffuse reflectance spectra of TiO_2 and P3HT/TiO_2 composites.

exhibiting an inverse relationship between reflectivity and wavelength, where a high reflectivity corresponds to a low absorbance, of TiO_2 and P3HT/TiO_2 composites (as presented in Fig. 7) were measured to determine their ability of harvesting light. As expected, TiO_2 reflects most light with a wavelength ranging from 400 nm to 800 nm and can only absorb UV light because of its wide band gap. However, in the spectrum of P3HT/TiO_2 composites, there are two absorption bands from 200 to 400 nm and from 400 to 800 nm, respectively. The former is assigned to the characteristic absorption of TiO_2 and the P3HT absorption band in the UV light region, while the latter is attributed to the electron transition from the valence bond to the antibonding polaron state of P3HT. In accordance with the absorption spectra of polymers (Fig. 2(b)), the visible light absorption range of C3 is slight wider than that of C1 and C2. In summary, there is no much difference in the ability of harvesting visible light among C1–C3 while TiO_2 can only absorb UV light.

3.3 Photocatalytic performance

The photocatalytic performance of TiO_2 and P3HT/TiO_2 composites C1–C3 was evaluated by using MO as target contaminant. It is documented that heterogeneous photocatalytic reactions occur at the surface rather than in the solution bulk and the pre-adsorption on the surface of photocatalyst is prerequisite for efficiently photocatalytic degradation of dyes [55]. Thus, the adsorption behaviors of the samples were carefully studied prior to the photocatalytic experiments and the adsorption efficiency of MO is presented in Fig. 8(a). The adsorption ratio of MO was defined as $(1 - C_t/C_0) \times 100\%$, where C_0 is the initial concentration of MO (10 mg/L), C_t is the concentration of MO at time t during the adsorption experiments. A negligible adsorption of MO is observed

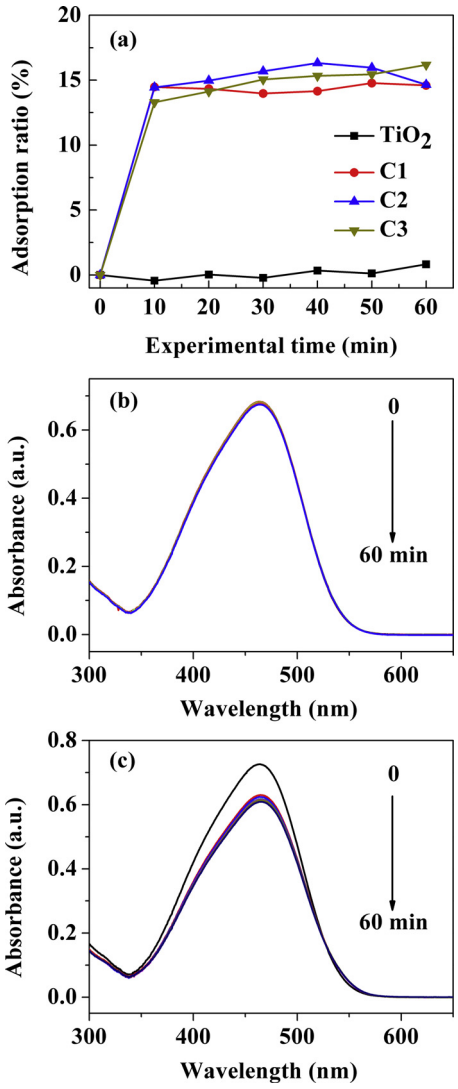

Fig. 8. (a) Adsorption ratio of MO vs. experimental time during the adsorption experiments in the presence of TiO_2 and P3HT/TiO_2 composites respectively. UV–vis absorption absorption spectra of MO with different time in the presence of (b) TiO_2 and (c) C3, correspondingly.

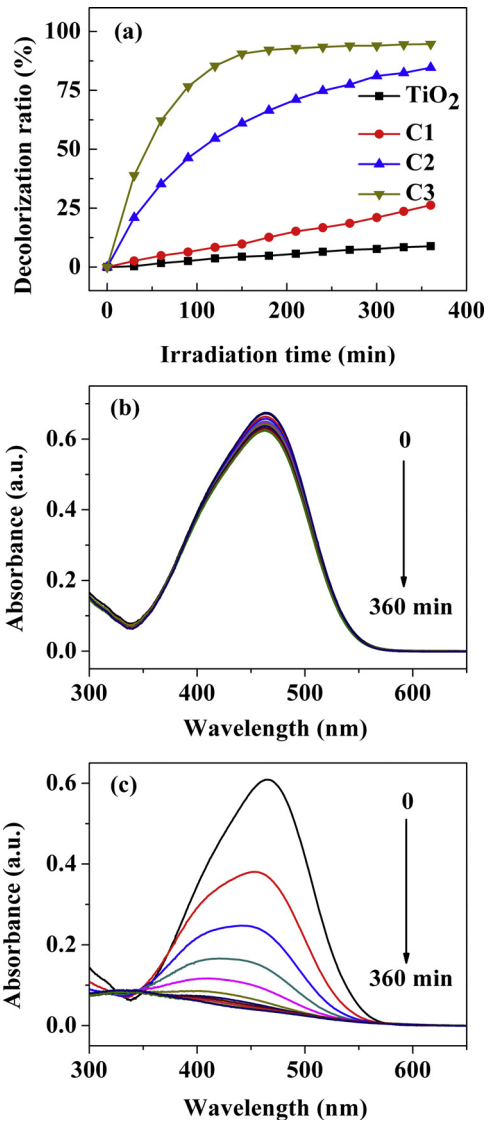

Fig. 9. (a) Degradation ratio of MO vs. irradiation time under visible light in the presence of TiO_2 and P3HT/TiO_2 composites, respectively. UV–vis absorption absorption spectra of MO with different time in the presence of (b) TiO_2 and (c) C3, correspondingly.

within 60 min in the presence of TiO_2 while the incorporation of P3HT into the composites provides an apparently additive effect on their adsorption capacities. For C1–C3, the adsorption–desorption equilibrium between the P3HT/TiO_2 composites and MO quickly reaches in 10 min with the adsorption ratio of about 15% which almost remains the same in the last 50 min. The UV–vis absorption spectra of MO with different time in the presence of TiO_2 remain the same basically (Fig. 8(b)) while that of C3 (Fig. 8(c)) show a decrease in absorbance with the increase of the experimental time and no peak wavelength shift was observed, confirming that the MO molecules were just adsorbed on the P3HT/TiO_2 composites. Compared to TiO_2, P3HT/TiO_2 composites show higher adsorption capacity toward MO, which will lead to the higher MO concentration around the catalyst, enhancing the interfacial reaction process of photoreaction and finally leading to higher photocatalytic activity. It is worth noting that C1–C3 exhibit almost the same adsorption capacity toward MO, which is attributable to their similar specific surface area (Table 2) and similar chemical structure of P1–P3, as well as their same content in composites.

The photocatalytic capability of TiO_2 and P3HT/TiO_2 composites under visible light illumination ($\lambda > 420$ nm) was evaluated by comparing the degradation efficiency of MO, as displayed in Fig. 9(a). The degradation ratio of MO was calculated as $(1 - C_t/C_0') \times 100\%$, where C_0' is the concentration of MO after adsorption, C_t is the concentration of MO at time t during the photocatalytic experiments. After 360 min of visible light irradiation, the degradation ratios of MO for TiO_2, C1 and C2 are 8.8%, 26.3% and 86.4%, respectively. As for C3, the degradation ratio of MO dramatically reaches 90.6% in 150 min illumination. Under visible light, TiO_2 can hardly degrade MO because of the limitation of wide band gap while P3HT/TiO_2 composites show more effective photocatalytic activity in an order of C3 > C2 > C1. It can be seen from Fig. 9(c) that with the increase of the irradiation time, the UV–vis absorption spectra of MO in the presence of C3 show not only a decrease in absorbance but also an obvious blue shift of the maximum absorption peak which is caused by the generation of intermediate products during the photodegradation of MO molecules [23]. Regardless of the generation of intermediate products during the photodegradation of MO molecules, the over diminution of absorbance is achieved with increasing irradiation

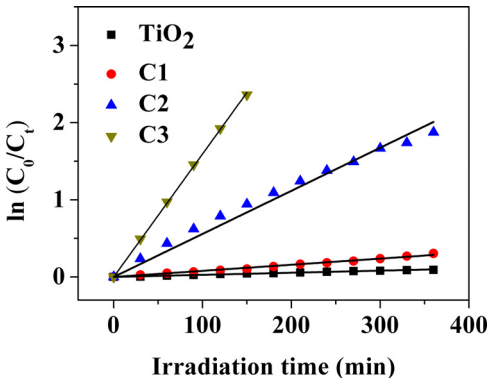

Fig. 10. Apparent first-order linear transform $\ln(C_0/C_t)$ of MO degradation kinetic plots for TiO_2 and P3HT/TiO_2 composites.

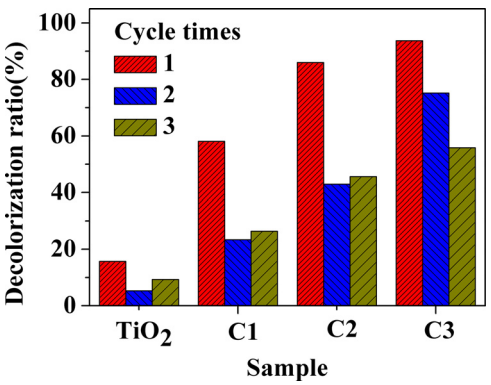

Fig. 11. Decolorization ratio of MO with TiO_2 and P3HT/TiO_2 composites in different recycling time.

Table 3
The kinetic constants of MO degradation for TiO_2 and P3HT/TiO_2 composites.

Catalysts	$k \times 10^3$ (min^{-1})	Correlation coefficient (r^2)
TiO_2	0.27	0.999
C1	0.79	0.997
C2	5.58	0.997
C3	15.94	0.994

time, indicating a further degradation of the residual intermediates until an ultimate dye mineralization.

To give quantifiable proof, the degradation of MO is found to accord with pseudo-first-order kinetics by linear transforms of $\ln(C_0'/C_t) = kt$, where C_0' is the concentration of MO after adsorption, C_t is the concentration of MO at time t and k is kinetic constant, as shown in Fig. 10. The corresponding kinetic constants (k) and correlation constants (r^2) for the fitted lines are given in Table 3. Under the same conditions, the kinetic constants of MO degradation for C1–C3 are 2.93, 20.67, 59.04 times as great as that for TiO_2, which shows the advantage of conjugated polymer/titanium dioxide hybrids for the degradation of organic pollutants under visible light. What is more, C2 and C3 exhibit significantly improved photocatalytic activity compared to C1, with kinetic constants 7.06 and 20.18 times as that of C1.

The photocatalytic activity of heterogeneous photocatalyst under visible light is mainly affected by three factors: the intensity of light absorbed, the separation efficiency of photogenerated charges under visible light irradiation and the interfacial reaction process. The reason why P3HT/TiO_2 composites show higher photocatalytic activity compared to TiO_2 can be assigned to (1) the promoted visible light absorption of P3HT/TiO_2, as demonstrated by the UV–vis diffuse reflectance spectra, (2) the higher separation efficiency facilitated by the heterojunction at the interfacial of TiO_2 and P3HT induced by the different energy level of them, which can lead to electron injection from π^*-orbital of P3HT to the conduction band of TiO_2, stopping from the regeneration of electron and hole and (3) the enhanced interfacial reaction process due to the higher MO concentration around catalyst because of the higher adsorption capacity of P3HT/TiO_2 composites (Fig. 8). However, it is surprise to find that there is a tremendous difference in photocatalytic activily of C1–C3 under visible light. In consideration of their similar ability of harvesting visible light (Fig. 7) and adsorption capacity toward MO (Fig. 8), the significantly improved phototalytic activity of C2 and C3 must be resulted from the introduction of cyanoacrylic acid moieties to P3HT as end-groups. It is well known that the covalent linkage between dyes and TiO_2 enables strong interfacial electronic coupling interaction between them and facilitates the efficient electron injection process for photovoltaics applications [39,40]. On the one hand, the introduction of cyanoacrylic acid moieties to P3HT as end-groups leads to the formation of ester bonds through reactions between carboxyl groups of end-group functionalized P3HT and hydroxyl groups on the surface of TiO_2. The resulted covalent linkage between P3HT and TiO_2 can give rise to close contact of the polymer chains with TiO_2, lead to strong interfacial electronic coupling interaction between them and facilitate electron injection from π^*-orbital of P3HT to the conduction band of TiO_2. On the other hand, the cyanoacrylic acid group, as an electron-accepting binding motif, will also encourage electron injection into the TiO_2 conduction band upon photoexcitation [51]. In the end, the facilitated electron injection from excited polymers to TiO_2 results in higher phototalytic activity of C2 and C3. Moreover, with an increase in the number of cyanoacrylic acid groups for the end of P3HT, the photocatalytic activity increases dramatically, confirming that the strong interaction is of great benefit to electron injection at the interfacial of P3HT and TiO_2.

3.4 Stability of the photocatalysts

To evaluate the photocatalytic stability of P3HT/TiO_2 composites, the photocatalysts were reused three times. Decolorization ratio of MO with TiO_2 and P3HT/TiO_2 composites in different recycling time is shown in Fig. 11. The decolorization ratio of MO decreases in the second cycle for TiO_2 and all the P3HT/TiO_2 composites compared with that in the first cycle while an unusual slightly increase is observed for all the samples in the third cycle except for C3 who shows a further decrease. There can be two main reasons for the reduction of decolorization ratio for samples toward MO, the loss of photocatalytic activity during the photocatalytic reaction and the residual MO molecules and intermediate products on the surface of photocatalysts in the previous cycling run, which would increase the concentration of MO solution and decrease the apparent decolorization ratio of MO. Based on the previous research, P3HT/TiO_2 composites possess excellent photocatalytic stability, losing their activity gradually and maintaining 60% of the degradation rate of MO of the first cycling run after 10 successive cycles under the visible light irradiation [25]. Furthermore, the loss of photocatalytic activity should be a gradual process. Therefore, the latter is more likely the main reason in consideration of the unusual increase for TiO_2, C1 and C2 in the third cycle because the residual molecules are saturated. For C3, Decolo rization ratio of MO reaches nearly 100% in the first cycle, resulting in less residual molecules on the surface of C3 and less decrease in the decolorization ratio in the second cycle compared with C1 and C2. The decoloration ratio decreases further in the third cycle due to more residual molecules in the second cycle. Anyway, the samples keep the decolorizaition ratio toward MO in an order of C3 > C2 > C1 > TiO_2 in each cycle, showing the advan-

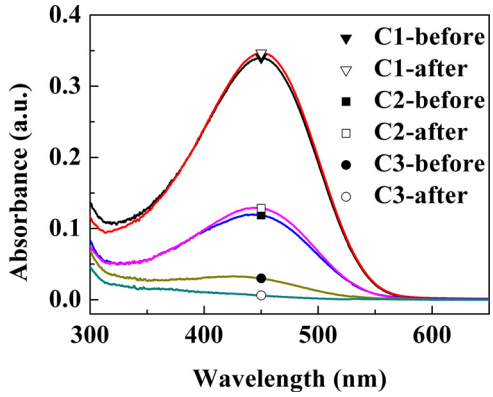

Fig. 12. UV–vis absorption spectra of P3HT solutions dissolved from P3HT/TiO_2 composites before and after three times photocatalytic degradation of MO.

tages incorporation of cyanoacrylic acid groups to the end of the P3HT.

In present study, we have focused on the enhacement of photocatalysis due to strong interaction between TiO_2 and end-group functionalizd P3HT, so the stability of their interaction should be paid special attention. Thus, dissolution tests for P3HT/TiO_2 composites before and after photocatalytic degradation of MO were carried out to confirm their photocatalytic stability. P3HT/TiO_2 composites (C1–C3) after three cycles were collected and added to a certain amount of chlorobenzene respectively. The mixtures, with concentration of 2 mg/mL, were kept in the dark for 10 h to dissolve polymers from composites. Same tests were done using P3HT/TiO_2 composites before photocatalystic reaction in the same time as comparisons. There is no much difference between the UV–vis absorption spectra of P3HT solutions dissolved from P3HT/TiO_2 composites before and after photocatalytic reaction, as displayed in Fig. 12, suggesting that the strong interaction in C2 and C3 is stability during photocatalytic degradation of MO and C2 and C3 possess considerable photocatalytic stability as C1.

4. Conclusion

In summary, by incorporation of cyanoacrylic acid groups to the end of the regioregular P3HT, which was subsequently bound to the surface of TiO_2, P3HT/TiO_2 composites with strong interfacial interaction were obtained. The strong interfacial interaction was demonstrated by results of X-ray photoelectron spectroscopy and dissolution tests. High-resolution transmission electron microscopy, nitrogen adsorption–desorption characterization and UV–vis diffuse reflectance spectra showed that all P3HT/TiO_2 composites, with pristine and end-group functionalized P3HT had similar morphology, specific surface area and ability of harvesting visible light. Their adsorption capacities were independent of end-group functionalization while their visible light photocatalytic activities were remarkably enhanced by an order of magnitude with the incorporation of cyanoarrylic acid end-groups and with an increase in the number of cyanoacrylic acid groups in the end of P3HT, the photocatalytic activity increased dramatically. This significantly enhanced photocatalytic activity benefits from the favored electron injection and facilitated separation of photogenerated carriers owing to the strong interfacial interaction between the end-group functionalized P3HT and TiO_2, suggesting the enormous role of interfacial interaction plays in the photocatalytic capability of conjugated polymer/TiO_2 photocatalysts. Also, the strong interfacial interaction has good stability and was not broken during three times photocatalytic degradation of MO. We believe this will open up a new pathway for design new efficient conjugated polymer/TiO_2 photocatalysts with great visible light photocatalytic activity.

Acknowledgment

The authors are grateful to the National Natural Science Foundation of China (grant No. 50573052 and No.51173116) for the support of this research.

References

[1] A. Fujishima, K. Honda, Nature 238 (1972) 37–38.
[2] A.A. Ismail, D.W. Bahnemann, Sol. Energy Mater. Sol. Cells 128 (2014) 85–101.
[3] Y. Ma, X.L. Wang, Y.S. Jia, X.B. Chen, H.X. Han, C. Li, Chem. Rev. 114 (2014) 9987–10043.
[4] C.-H. Kuo, W. Li, L. Pahalagedara, A.M. El-Sawy, D. Kriz, N. Genz, C. Guild, T. Ressler, S.L. Suib, J. He, Angew. Chem. 127 (2015) 2375–2380.
[5] S.W. Leong, A. Razmjou, K. Wang, K. Hapgood, X.W. Zhang, H.T. Wang, J. Membr. Sci. 472 (2014) 167–184.
[6] J.H. Carey, J. Lawrence, H.M. Tosine, Bull. Environ. Contam. Toxicol. 16 (1976) 697–701.
[7] A.L. Pruden, D.F. Ollis, J. Catal. 82 (1983) 404–417.
[8] M. Muruganandham, R.P.S. Suri, M. Sillanpaa, J.J. Wu, B. Ahmmad, S. Balachandran, M. Swaminathan, J. Nanosci. Nanotechnol. 14 (2014) 1898–1910.
[9] H.L. Wang, L.S. Zhang, Z.G. Chen, J.Q. Hu, S.J. Li, Z.H. Wang, J.S. Liu, X.C. Wang, Chem. Soc. Rev. 43 (2014) 5234–5244.
[10] J. Schneider, M. Matsuoka, M. Takeuchi, J.L. Zhang, Y. Horiuchi, M. Anpo, D.W. Bahnemann, Chem. Rev. 114 (2014) 9919–9986.
[11] T.L. Thompson, J.T. Yates Jr., Chem. Rev. 106 (2006) 4428–4453.
[12] W.W.H. Wong, J. Subbiah, S.R. Puniredd, W. Pisula, D.J. Jones, A.B. Holmes, Polym. Chem.-U.K. 5 (2014) 1258–1263.
[13] S. Ren, R. Dawson, D.J. Adams, A. Cooper, Polym. Chem.-U.K. 4 (2013) 5585–5590.
[14] S. Chu, C. Wang, Y. Yang, Y. Wang, Z. Zou, RSC Adv. 4 (2014) 57153–57158.
[15] Z. Fang, A.A. Eshbaugh, K.S. Schanze, J. Am. Chem. Soc. 133 (2011) 3063–3069.
[16] H. Jiang, X. Zhao, A.H. Shelton, S.H. Lee, J.R. Reynolds, K.S. Schanze, ACS Appl. Mater. Interfaces 1 (2009) 381–387.
[17] M. Jeffries-El, G. Sauve, R.D. McCullough, Adv. Mater. 16 (2004) 1017.
[18] R.H. Lohwasser, J. Bandara, M. Thelakkat, J. Mater. Chem. 19 (2009) 4126–4130.
[19] S. Gunes, H. Neugebauer, N.S. Sariciftci, Chem. Rev. 107 (2007) 1324–1338.
[20] T.-P. Nguyen, Surf. Coat. Technol. 206 (2011) 742–752.
[21] Y.-W. Su, W.-H. Lin, Y.-J. Hsu, K.-H. Wei, Small (Weinheim an der Bergstrasse Germany) 10 (2014) 4427–4442.
[22] Y.F. Zhu, S.B. Xu, L. Jiang, K.L. Pan, Y. Dan, React. Funct. Polym. 68 (2008) 1492–1498.
[23] Y.F. Zhu, Y. Dan, Sol. Energy Mater. Sol. Cells 94 (2010) 1658–1664.
[24] S. Xu, L. Gu, K. Wu, H. Yang, Y. Song, L. Jiang, Y. Dan, Sol. Energy Mater. Sol. Cells 96 (2012) 286–291.
[25] D. Wang, J. Zhang, Q. Luo, X. Li, Y. Duan, J. An, J. Hazard. Mater. 169 (2009) 546–550.
[26] D. Wang, Y. Wang, X. Li, Q. Luo, J. An, J. Yue, Catal. Commun. 9 (2008) 1162–1166.
[27] X. Li, G. Jiang, G. He, W. Zheng, Y. Tan, W. Xiao, Chem. Eng. J. 236 (2014) 480–489.
[28] G. Liao, S. Chen, X. Quan, Y. Zhang, H. Zhao, Appl. Catal. B: Environ. 102 (2011) 126–131.
[29] M.A. Salem, A.F. Al-Ghonemiy, A.B. Zaki, Appl. Catal. B: Environ. 91 (2009) 59–66.
[30] H. Zhang, R. Zong, J. Zhao, Y. Zhu, Environ. Sci. Technol. 42 (2008) 3803–3807.
[31] C. Wen, K. Hasegawa, T. Kanbara, S. Kagaya, T. Yamamoto, J. Photochem. Photobiol. A 137 (2000) 45–51.
[32] L. Song, R. Qiu, Y. Mo, D. Zhang, H. Wei, Y. Xiong, Catal. Commun. 8 (2007) 429–433.
[33] B. Muktha, D. Mahanta, S. Patil, G. Madras, J. Solid State Chem. 180 (2007) 2986–2989.
[34] S. Ameen, M.S. Akhtar, Y.S. Kim, H.S. Shin, Appl. Catal. B: Environ. 103 (2011) 136–142.
[35] F. Deng, L. Min, X. Luo, S. Wu, S. Luo, Nanoscale 5 (2013) 8703–8710.
[36] M.K. Nazeeruddin, A. Kay, I. Rodicio, R. Humphry-Baker, E. Mueller, P. Liska, N. Vlachopoulos, M. Graetzel, J. Am. Chem. Soc. 115 (1993) 6382–6390.
[37] Y.G. Kim, J. Walker, L.A. Samuelson, J. Kumar, Nano Lett. 3 (2003) 523–525.
[38] J.S. Liu, E.N. Kadnikova, Y.X. Liu, M.D. McGehee, J.M.J. Frechet, J. Am. Chem. Soc. 126 (2004) 9486–9487.
[39] A. Mishra, M.K.R. Fischer, P. Baeuerle, Angew. Chem. Int. Ed. 48 (2009) 2474–2499.
[40] P. Ganesan, A. Chandiran, P. Gao, R. Rajalingam, M. Graetzel, M.K. Nazeeruddin, J. Phys. Chem. C 118 (2014) 16896–16903.
[41] S.B. Mane, C.-H. Hung, New J. Chem. 38 (2014) 3960–3972.
[42] R. Stalder, D. Xie, A. Islam, L. Han, J.R. Reynolds, K.S. Schanze, ACS Appl. Mater. Interfaces 6 (2014) 8715–8722.

[43] K. Neuthe, F. Bittner, F. Stiemke, B. Ziem, J. Du, M. Zellner, M. Wark, T. Schubert, R. Haag, Dyes Pigm. 104 (2014) 24–33.
[44] H. Honda, T. Matsumoto, R. Tamura, K. Kanaizuka, A. Kobayashi, M. Kato, M.-A. Haga, H.-C. Chang, Chem. Lett. 43 (2014) 1189–1191.
[45] G. Guerrero, P.H. Mutin, A. Vioux, Chem. Mater. 13 (2001) 4367–4373.
[46] B.J. Brennan, A.E. Keirstead, P.A. Liddell, S.A. Vail, T.A. Moore, A.L. Moore, D. Gust, Nanotechnology 20 (2009) 1–10.
[47] P. Huang, Z. Li, J. Lin, D. Yang, G. Gao, C. Xu, L. Bao, C. Zhang, K. Wang, H. Song, H. Hu, D. Cui, Biomaterials 32 (2011) 3447–3458.
[48] R. Rahimi, M.M. Moghaddas, S. Zargari, J. Sol–Gel Sci. Technol. 65 (2013) 420–429.
[49] T. Kamegawa, Y. Masuda, N. Suzuki, Y. Horiuchi, H. Yamashita, ACS Appl. Mater. Interface 3 (2011) 4561–4565.
[50] R.S. Loewe, S.M. Khersonsky, R.D. McCullough, Adv Mater. 11 (1999) 250–253.
[51] R.A. Kr€uger, T.J. Gordon, T. Baumgartner, T.C. Sutherland, Appl. Mater. Interfaces 3 (2011) 2031–2041.
[52] Y. Wang, M. Zhong, F. Chen, J. Yang, Appl. Catal. B: Environ. 90 (2009) 249–254.
[53] R.P. Netterfield, P.J. Martin, C.G. Pacey, W.G. Sainty, D.R. McKenzie, G. Auchterlonie, J. Appl. Phys. 66 (1989) 1805–1809.
[54] D.V. Brazhnyk, Y.P. Zaitsev, I.V. Bacherikova, V.A. Zazhigalov, J. Stoch, A. Kowal, Appl. Catal. B: Environ. 70 (2007) 557–566.
[55] W. Dong, C.W. Lee, X. Lu, Appl. Catal. B: Environ. 95 (2010) 197–207.